Keynote Lecture, **International Thermal Science Seminar - ITSS II, ASME-ICHMT-ZSIS**,
(eds: Bergles, A. E., Golobic, I., Amon, C. H. and Bejan, A.), Bled, Slovenia, June 13-16, 2004, pp. 133-144.

Convective Heat Transfer Control Using Magnetic and Electric Fields

George S. Dulikravich[1*], Marcelo J. Colaço[2]

[1]*Department of Mechanical & Materials Eng., Florida International University, 10555 West Flagler Street, Miami, Florida 33174, U.S.A., *dulikrav@fiu.edu*
[2]*Department of Mechanical Engineering, EE/COPPE, Federal University of Rio de Janeiro, UFRJ, Cidade Universitaria, Caixa. Postal 68503, Rio de Janeiro, RJ, 21945-970, Brazil*

Abstract

A practical approach to non-intrusively controlling electrically conducting melt flow-fields and heat transfer could be achieved by using externally applied magnetic and electric fields. Computational methods are needed to enhance our understanding of this phenomena and its potential in practical industrial processes. In addition, numerical simulation can be used together with optimization to determine distributions of magnets and/or electrodes on the walls of a container with an electrically conducting fluid so that the resulting Lorentz forces will affect the flow throughout the domain or in desired regions only, so that desired thermal gradients could be maintained and desired solid/melt interface topology could be created and preserved during unsteady solidification.

Implicit numerical algorithms were developed and used in this research to integrate equations of classical magnet-hydro-dynamics and classical electro-hydro-dynamics. The algorithms utilized finite volume method and a hybrid optimizer with automatic switching among different optimization modules. Both algorithms were used to develop accurate computer codes for prediction and optimization of solidification from a melt under the influence of externally applied magnetic and electric fields. The objective was to find such distributions of intensities of wall-mounted magnets and electrodes that will create desired features of the flow-field or melt/solid interface topology. The computational results indicate significantly different flow-field patterns and thermal fields in the melt and the accrued solid in the cases of externally applied optimized magnetic and electric fields. This clearly suggests the possibility of developing smart manufacturing protocols for creating objects that will have functionally graded physical properties.

Introduction

It has been well-known that fluid flow, thus convective heat transfer, could be influenced if the electrically conducting fluid is subjected to either magnetic or electric or combined fields. This concept has been used for decades in electromagnetic stirring of molten metals, electrophoretic separation and filtration processes, magneto-hydro-dynamic pumping and electro-hydro-dynamic pumping, etc. [1-9]. However, mathematical models allowing for detailed understanding of the interaction of the electric, magnetic, thermal, gravitational and pressure fields has not been available until relatively recently [10-13]. Numerical simulation of such processes using these advanced models is still unavailable because of the unavailability of the large number of physical properties that still need to be evaluated experimentally [10, 13].

Consequently, the complete EMHD model has been solved for only simple problems. Actually, EMHD has traditionally been divided into two overly simplified sub-models: magneto-hydro-dynamics (MHD) and electro-hydro-dynamics (EHD). MHD models incompressible fluid flows under the influence of an externally imposed magnetic field, while neglecting any electric fields and electrically charged particles. EHD models incompressible fluid flows under the influence of an externally imposed electric field, while neglecting any magnetic fields.

These simplified analytical sub-models of the EMHD have recently been used in the attempts to numerically simulate separate MHD and EHD involving heat transfer and to attempt to demonstrate feasibility of solving inverse problems in convection involving optimized magnetic and electric fields [14-21].

[*]Adapted from "Instructions for Manuscript Preparations" for ITSS I and Elsevier's "Gateway guide for authors".

Nomenclature

b	electric charge mobility
$\mathbf{B}$	magnetic field vector
B_x	magnetic flux component in x-direction
B_y	magnetic flux component in y-direction
C_P	specific heat at constant pressure
D_e	electric charge diffusion coefficient
$\mathbf{E}$	electric field vector
E_x	electric field component in x-direction
E_y	electric field component in y-direction
f	solid fraction in a fluid/solid mixture
$\boldsymbol{g}$	acceleration of the gravity
h	enthalpy per unit mass
$\mathbf{J}$	total electric current density vector
k	thermal conductivity
L	latent heat of solidification/melting
n	partition coefficient in Sheil's equation (Eq. 5)
p	pressure
q_e	local free electric charge per unit volume
Ra	Rayleigh number
t	time
T	temperature
u	velocity component in x-direction
v	velocity component in y-direction
x, y	Cartesian coordinates

Greek letters

β	thermal expansion coefficient
ε_0	vacuum electric permittivity
φ	electric potential
μ	fluid viscosity
μm	magnetic permeability
σ	electric conductivity

Subscripts

h	hot surface
c	cold surface
l	liquid value
s	solid value

Melting/solidification phase change model

In this paper we used the enthalpy method [22] to deal with the phase change problem. In this method, the energy equation appears as a mixed enthalpy-temperature equation. Thus, we must obtain some relationship between the temperature and the enthalpy to be used in the energy equation.

For the case of a binary alloy, if $h < h_{\text{solid}}$, we have

$$T = \frac{h}{C_{Ps}} \tag{1}$$

or, if $h > h_{\text{liquid}}$

$$T = \frac{(C_{Pl} - C_{Ps})T_s - L + h}{C_{Pl}} \tag{2}$$

For the case of mixture, we have a range of temperatures where the solidification might occur. Thus, if $h_{\text{solid}} < h < h_{\text{liquid}}$,

$$T = \frac{(1-f)[(C_{Pl} - C_{Ps})T_s - L] + h}{C_{Pl} - f(C_{Pl} - C_{Ps})} \tag{3}$$

The solid fraction f is given by the Scheil's model [23]

$$f = 1 - \left(\frac{T - T_s}{T_l - T_s}\right)^{1/(n-1)} \tag{4}$$

In the above equation, we set the partition coefficient $n = 2$, which reduces the Scheil's model to the linear interpolation function. Note that if $T < T_{\text{solid}}$, f must be set to unity and, if $T > T_{\text{liquid}}$, f must be set to zero.

The magnetic, electric and thermal properties were approximated as linear functions within the mushy region ($T_{\text{solid}} < T < T_{\text{liquid}}$) and kept constants within each phase. Thus, in the mushy region

$$\psi = f\psi_s + (1-f)\psi_l \tag{5}$$

where ψ represents the density, thermal conductivity, viscosity, magnetic permeability and electric conductivity. For the viscosity of the solid phase we used

$$\frac{\mu_s}{\mu_l} \geq 10^6 \tag{6}$$

Note that this formulation implicitly introduces rapidly increased viscous dissipation inside the mushy region thus creating a similar effect as if using a considerably more complicated of a porous flow dissipation in the mushy region. Furthermore, this formulation allows a typical computational fluid dynamics code to simultaneously predict liquid and solid phases in the mixture flow whereby the solid phase is treated as the second fluid phase with an extremely high viscosity.

For the specific heat at constant pressure within the mushy region, we used the thermodynamic property [22]

$$C_P = \frac{\partial h}{\partial T} \approx \frac{\sqrt{\left(\frac{\partial h}{\partial x}\right)^2 + \left(\frac{\partial h}{\partial y}\right)^2}}{\sqrt{\left(\frac{\partial T}{\partial x}\right)^2 + \left(\frac{\partial T}{\partial y}\right)^2}} \tag{7}$$

When dealing with a mixture, the enthalpy is a function of the temperature, which is a function of the solid fraction which is itself a function of the temperature. Thus, if h_{solid}

*Adapted from "Instructions for Manuscript Preparations" for ITSS I and Elsevier's "Gateway guide for authors".

$< h < h_{\text{liquid}}$, we must solve a non-linear system for T. From Eqs. (3) and (4) we have

$$T - \frac{\left(\frac{T-T_s}{T_l-T_s}\right)^{1/(n-1)}\left[(C_{Pl}-C_{Ps})T_s - L\right] + h}{C_{Pl} - \left[1-\left(\frac{T-T_s}{T_l-T_s}\right)^{1/(n-1)}\right](C_{Pl}-C_{Ps})} = 0 \tag{8}$$

This equation can be solved for local temperature, T, by the secant method.

Notice also that according to Boussinesq approximation the energy source term resulting from viscous dissipation is neglected and buoyancy effects are accounted only in the vertical component of the linear momentum balance.

Magneto-hydro-dynamics (MHD) model

Typical formulation for the laminar MHD natural convection of an incompressible Newtonian fluid involves conservation laws for mass, momentum and energy and a magnetic field transport equation [7].

$$\nabla \cdot \mathbf{v} = 0 \tag{9}$$

$$\rho \frac{D\mathbf{v}}{Dt} = -\rho \mathbf{g}\left[1-\beta(T-T_o)\right] - \nabla p + \nabla \cdot \left[\mu\left(\nabla \mathbf{v} + \nabla \mathbf{v}^*\right)\right] + \left(\nabla \times \frac{\mathbf{B}}{\mu_m}\right) \times \mathbf{B} \tag{10}$$

$$\rho C_P \frac{DT}{Dt} = \nabla \cdot (k \nabla T) + \frac{1}{\sigma}\left(\nabla \times \frac{\mathbf{B}}{\mu_m}\right) \cdot \left(\nabla \times \frac{\mathbf{B}}{\mu_m}\right) \tag{11}$$

When there is no imposed electric field ($\mathbf{E} = 0$), no polarization, no magnetization due to circulation of charges, no Seebeck effect, no electric charge diffusion, no free electric charge, and when fluid is incompressible and with constant electric conductivity, the general magnetic field transport equation assumes the familiar form

$$\frac{\partial \mathbf{B}}{\partial t} - \nabla \times \left(\mathbf{v} \times \mathbf{B}\right) = \frac{1}{\mu_m \sigma} \nabla^2 \mathbf{B} \tag{12}$$

These equations can be cast into the following general system

$$\frac{\partial Q}{\partial t} + \frac{\partial E}{\partial x} + \frac{\partial F}{\partial y} = S \tag{13}$$

where

$$Q = \lambda \phi \tag{14}$$

$$E = \lambda u \phi^* - \Gamma \frac{\partial \phi^{***}}{\partial x} \tag{15}$$

$$F = \lambda v \phi^{**} - \Gamma \frac{\partial \phi^{***}}{\partial y} \tag{16}$$

The values of S, λ, ϕ, ϕ^*, ϕ^{**},ϕ^{***} and Γ are given in Table 1 for the equations of conservation of mass, x-momentum, y-momentum, energy, magnetic flux in the x-direction and magnetic flux in the y-direction.

These equations were transformed from the physical Cartesian (x,y) coordinates to the computational coordinate system (ξ,η) and solved by the finite volume method. The implicit SIMPLEC method [24] was used to solve velocity-pressure coupling problem. The WUDS interpolation scheme [25] was used to obtain the values of u, v, h, B_x and B_y as well as their derivatives at the interfaces of each control volume. The resulting linear system was solved by the GMRES method.

Table 1. Parameters for the Navier-Stokes and Maxwell equations in a standard MHD model.

Conservation of	λ	ϕ	ϕ^*	ϕ^{**}	ϕ^{***}	Γ	S
Mass	ρ	1	1	1	1	0	0
x-momentum	ρ	u	u	u	u	μ	$-\frac{\partial p}{\partial x} - \frac{B_y}{\mu_m}\left[\frac{\partial B_y}{\partial x} - \frac{\partial B_x}{\partial y}\right]$
y-momentum	ρ	v	v	v	v	μ	$-\frac{\partial p}{\partial y} - \rho g\left[1-\beta(T-T_o)\right] + \frac{B_x}{\mu_m}\left[\frac{\partial B_y}{\partial x} - \frac{\partial B_x}{\partial y}\right]$
Energy	ρ	h	h	h	T	k	$\frac{1}{\sigma \mu_m^2}\left[\frac{\partial B_y}{\partial x} - \frac{\partial B_x}{\partial y}\right]^2$
Magnetic flux in x-direction	1	B_x	0	B_x	B_x	$\frac{1}{\mu_m \sigma}$	$\frac{\partial (u B_y)}{\partial y}$
Magnetic flux in y-direction	1	B_y	B_y	0	B_y	$\frac{1}{\mu_m \sigma}$	$\frac{\partial (v B_x)}{\partial x}$

Electro-hydro-dynamics (EHD) model

A typical model for laminar EHD natural convection of a Newtonian fluid involves conservation of mass, linear momentum, energy, electric charge conservation and electric charge transport equations. The energy source term resulting from viscous dissipation is neglected and buoyancy effects are approximated by the Boussinesq hypothesis. Then the Navier-Stokes and Maxwell equations for non-polarizable fluids are [7]

$$\nabla \cdot \mathbf{v} = 0 \tag{17}$$

$$\rho \frac{D\mathbf{v}}{Dt} = -\rho \mathbf{g}\left[1 - \beta\left(T - T_o\right)\right] - \nabla p + \nabla \cdot \left[\mu\left(\nabla \mathbf{v} + \nabla \mathbf{v}^*\right)\right] + q_e \mathbf{E} \tag{18}$$

$$\rho C_P \frac{DT}{Dt} = \nabla \cdot \left[k \nabla T\right] + \mathbf{J} \cdot \mathbf{E} \tag{19}$$

$$\nabla \cdot \left(\varepsilon_o \mathbf{E}\right) = q_e \tag{20}$$

$$\frac{\partial q_e}{\partial t} + \nabla \cdot \mathbf{J} = 0 \tag{21}$$

where the total current can be formulated as

$$\mathbf{J} = q_e (b\,\mathbf{E} + \mathbf{v}) - D_e \nabla q_e \tag{22}$$

Notice that electric conductivity and charge mobility are related as

$$\sigma = q_e b \tag{23}$$

When electric fields are in the 10^4 to 10^5 volts cm^{-1} range, the charge difusion contribution will be very small, except when gradients occur over lengths of the order less than 10^{-6} cm [7]. Under the action of the electrical field, the charge carriers of mobility b migrate with a velocity $b\mathbf{E}$, $\mathbf{E}$ being the field modified by the space-charge density q_e. Since the electric field is irrotational, it follows that

$$\mathbf{E} = -\nabla \varphi \tag{24}$$

where φ is the electric potential. Thus, from equation (1.a), we have

$$\nabla^2 \varphi = -\frac{q_e}{\varepsilon_o} \tag{25}$$

The complete system of Navier-Stokes and Maxwell equations can be written then as

$$\frac{\partial Q}{\partial t} + \frac{\partial E}{\partial x} + \frac{\partial F}{\partial y} = S \tag{26}$$

where

$$Q = \lambda \phi \tag{27}$$

$$E = \left(\lambda u + \zeta E_x\right)\phi^* - \Gamma \frac{\partial \phi^{***}}{\partial x} \tag{28}$$

$$F = \left(\lambda v + \zeta E_y\right)\phi^{**} - \Gamma \frac{\partial \phi^{***}}{\partial y} \tag{29}$$

The values of S, λ, ζ, ϕ, ϕ^*, ϕ^{**},ϕ^{***} and Γ are given in Table 1 for the equations of conservation of mass, x-momentum, y-momentum, energy, electric potential and electric charged particles distribution.

The above equations were transformed from the physical to the computational coordinate system (ξ,η) and solved by the finite volume method. The SIMPLEC Method [24] was used to solve the velocity-pressure coupling problem implicitly. The WUDS interpolation scheme [25] was used to obtain the values of u, v, h, φ and q_e as well as their derivatives at the interfaces of each control volume. The resulting linear system was solved by the GMRES method.

Table 2. Parameters for the Navier-Stokes and Maxwell equations in a standard EHD model.

Conservation of	λ	ζ	ϕ	ϕ^*	ϕ^{**}	ϕ^{***}	Γ	S
Mass	ρ	0	1	1	1	1	0	0
x-momentum	ρ	0	u	u	u	u	μ	$-\frac{\partial p}{\partial x} + q_e E_x$
y-momentum	ρ	0	v	v	v	v	μ	$-\frac{\partial p}{\partial y} - \rho g\left[1 - \beta\left(T - T_o\right)\right] + q_e E_y$
Energy	ρ	0	h	h	h	T	k	$q_e\left[b\left(E_x^2 + E_y^2\right) + uE_x + vE_y\right] - D_e\left(E_x \frac{\partial q_e}{\partial x} + E_y \frac{\partial q_e}{\partial y}\right)$
Electric potential	0	0	0	0	0	φ	-1	$-\frac{q_e}{\varepsilon_o}$
Electric charged particles transport	1	b	q_e	q_e	q_e	q_e	D_e	0

Optimization of magnetic and electric fields

The hybrid optimization algorithm [26] utilized in this work incorporates some of the most popular optimization modules: genetic algorithm, a quasi-Newton Pschenichny-Danilin algorithm, modified Nelder-Mead simplex algorithm, sequential quadratic programming algorithm, Davidon-Fletcher-Powell gradient search algorithm, and differential evolution algorithm. Each of these modules provides a unique approach to optimization with varying degrees of convergence, reliability and robustness at different cycles during the iterative optimization procedure. A set of analytically formulated heuristic switching criteria were coded into the program to automatically switch back and forth among the different optimization modules as the iterative minimization process proceeds [26].

The evolutionary hybrid algorithm handles the existence of equality and inequality constraint functions in three ways: Rosen's projection method, feasible searching, and random design generation. Rosen's projection method provided search directions that guided descent-directions tangent to active constraint boundaries. In the feasible search, designs that violated constraints were automatically restored to feasibility via the minimization of the active global constraint functions. If at any time this constraint minimization failed, random designs were generated about the current design until a new feasible design was reached.

Gradients of the objective and constraint functions with respect to the design variables, also called design sensitivities, were calculated using finite differencing formulas. The population matrix was updated every iteration with new designs and ranked according to the value of the objective function. Whenever the optimization process detects that it is terminating in a local minimum, then currently used optimization module is automatically switched to another optimization module thus escaping from the local minimum. The optimization problem was completed when the maximum number of iterations or objective function evaluations were exceeded, or when the optimization program tried all individual optimization modules, but failed to produce a non-negligible decrease in the objective function. The latter criterion was the primary qualification of convergence, and it usually indicated that a global minimum had been found.

Numerical experiments

The first objective of this work was to develop and validate MHD and EHD analysis codes in cases involving convection heat transfer without and with solidification. The second objective was to combine these analysis codes and an optimization algorithm in order to determine the appropriate variations of strength of the magnetic and electric fields along the boundaries of a container with a fluid that will create desired flow-field and the solid/melt interface topology. As a by-product of the solution of this *de facto* inverse problem, appropriate variations of heat fluxes along the boundary of the container could be found. These types of inverse MHD and EHD problems have a significant potential in actively controlling the natural convection effects thus possibly producing solids with desired shapes having lower thermal stresses and lower and more uniform distribution of impurities than those obtained in a presence of very strong buoyancy forces.

MHD test cases

First, let us demonstrate the inverse determination of the magnetic boundary conditions that create certain pre-specified flow-field within some domain. Figure 1 shows the geometry and the boundary conditions for the test cases considered here.

The height and length of the square container were equal to 0.15 m. The top and bottom walls were kept thermally insulated. The left boundary was kept at a "hot" temperature while the right wall was kept at a "cold" temperature. For the first test case [19,20], there was no phase change, since the "hot" and "cold" temperatures were above the melting temperature.

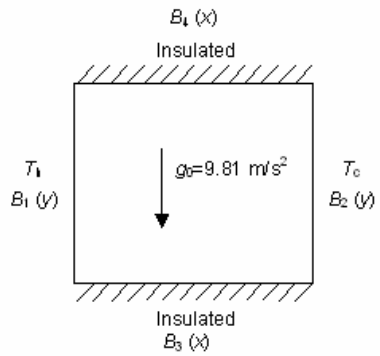

Figure 1. Geometry and boundary conditions for MHD.

The four walls were subjected to unknown magnetic field distributions whose directions were made orthogonal to each wall. In order to satisfy the magnetic flux conservation equation

$$\nabla \bullet \mathbf{B} = 0 \tag{30}$$

the following periodic conditions were imposed

$$B_1(y) = B_2(y) \tag{31}$$

$$B_3(x) = B_4(x) \tag{32}$$

The objective was to minimize the natural convection effects by reducing the gradient of temperature along the *y* direction, thus trying to obtain a temperature profile similar to those obtained for pure conduction. The objective function to be minimized is then formulated as [19,20]

$$F = \sqrt{\frac{1}{\#cells}\sum_{i=1}^{\#cells}\left(\frac{\partial T_i}{\partial y_i}\right)^2} \tag{33}$$

The magnetic field boundary conditions were inversely determined at either four or six points equally spaced along each of the four boundaries and interpolated using B-splines for the other points at those boundaries. The magnetic boundary conditions at $x = 0.15$ m and $y = 0.15$ m were then obtained using periodic conditions from Eq. (31) and Eq. (32).

The fluid analyzed was silicon [19,20]. For the first test case, the temperature difference T_h-T_c was set equal to 0.654351 K, which gives a Rayleigh number of 10^5.

Figure 2 shows streamlines, isotherms and heat fluxes on all four boundaries predicted without any magnetic flux applied and no phase change (left column) and streamlines, isotherms and heat fluxes on all four boundaries resulting from the magnetic boundary conditions optimized using six points on each boundary. One can see that the gradients of temperature in the y direction are reduced. Figure 3 shows the optimized magnetic field boundary conditions for $x = 0$ and $y = 0$ and Figure 4 shows the convergence history of the process. One can see that the differential evolution algorithm did almost all the work.

As a second test case, we minimized the curvature of the isotherms in a solidifying process after a pre-specified time from the start of the solidifying process. The temperature difference T_h-T_c was set equal to 6.54351 K (T_h = 1686.04351 K, T_c = 1676.5 K) and the length of the square container was taken as 0.069624 m, which gives a Rayleigh number of 10^5. The solidus and liquidus temperatures were equal to 1681.0 K and 1686.0 K, respectively. Thus, a mushy region exists between the phases. The initial condition was set as $T_0 = T_h$. Then, the solidifying process started at the right wall, where $T = T_c$.

Figure 5 shows the streamlines, isotherms and heat fluxes on all four boundaries for this test case without any magnetic flux applied, predicted at 500 seconds, (left column) as well as the streamlines, isotherms and heat fluxes on all four boundaries resulting from optimization of six B-spline points for the estimation of the magnetic boundary conditions on each boundary (right column). The boundary conditions at the other points were interpolated using B-splines. One can see that the curvature of the isotherms is smaller than in the case without any magnetic fields applied.

Figure 6 shows the optimized variation of the magnetic fields orthogonal to $x = 0$ and $y = 0$ boundaries. Figure 7 shows the convergence history of the optimization process. Genetic algorithm module did most of the work.

EHD test cases

In another test case we dealt with the inverse determination of the electric boundary conditions that create some pre-specified flow-field features within some region [21]

The height and length of the closed container filled with the electrically conducting liquid were equal to 33.33 mm and 66.67 mm, respectively. The vertical walls were kept thermally insulated. The bottom boundary was kept at a "hot" temperature while the top wall was kept at a "cold" temperature. A slightly triangular temperature profile was applied to the bottom wall in order to create a preferential direction for the thermally induced fluid flow.

The vertical walls were subjected to unknown electric potential boundary conditions. The electric charged particles were assumed to enter the fluid from the walls where the electric potential was applied. The objective was to minimize the natural convection effects by reducing the gradient of temperature along the x direction, thus trying to obtain a temperature profile similar to those obtained for pure conduction. The objective function to be minimized was then formulated as

$$F = \sqrt{\frac{1}{\#cells}\sum_{i=1}^{\#cells}\left(\frac{\partial T_i}{\partial x_i}\right)^2} \tag{34}$$

The electric boundary conditions were inversely determined at six points equally spaced along each of the vertical walls and parameterized using B-splines for the other points of these boundaries. In this case we considered natural convection of gallium arsenide [21]. The temperature difference T_h-T_c was set equal to 1.0 K, which gives a Rayleigh number of 1.9×10^4.

For the first test case, there was no phase change, since the "hot" and "cold" temperatures were above the melting temperature (T_h = 1521.5 K; T_c = 1520.5 K).

Figure 8 shows the streamlines, isotherms and heat fluxes on all four walls predicted for the first test case without any electric field applied and no phase change (left column). Figure 8 also shows the streamlines, isotherms, and heat fluxes on the four walls when using six points on each vertical wall for the estimation of the electric boundary conditions (right column). One can see that the gradients of temperature in the x direction are reduced close to the top and bottom walls. One can see that the isotherms start to become horizontal which is similar to those obtained if the gravity vector were acting in the horizontal direction.

Figure 9 shows the optimized electric potential and Fig. 10 shows the convergence history, where the DFP and genetic algorithm modules did all the work.

In a second test case, we tried to minimize the curvature of the isotherms in a solidifying process after a pre-specified time from the start of the solidifying process. Figure 11 shows (left column) the results obtained for a Rayleigh number equal to 1.9×10^4 without any electric field applied. In this case, the "hot" and "cold" temperatures were equal to 1510.5 K and 1511.5 K, respectively.

Figure 11 also shows the results obtained with an optimized electric potential acting in the horizontal direction. Note that the isotherms are smoother than those for a case without any electric field applied.

Figure 12 shows the optimized electric potential and Fig. 13 shows the convergence history for the hybrid optimizer. Note that the differential evolution module did almost all the work for this test case.

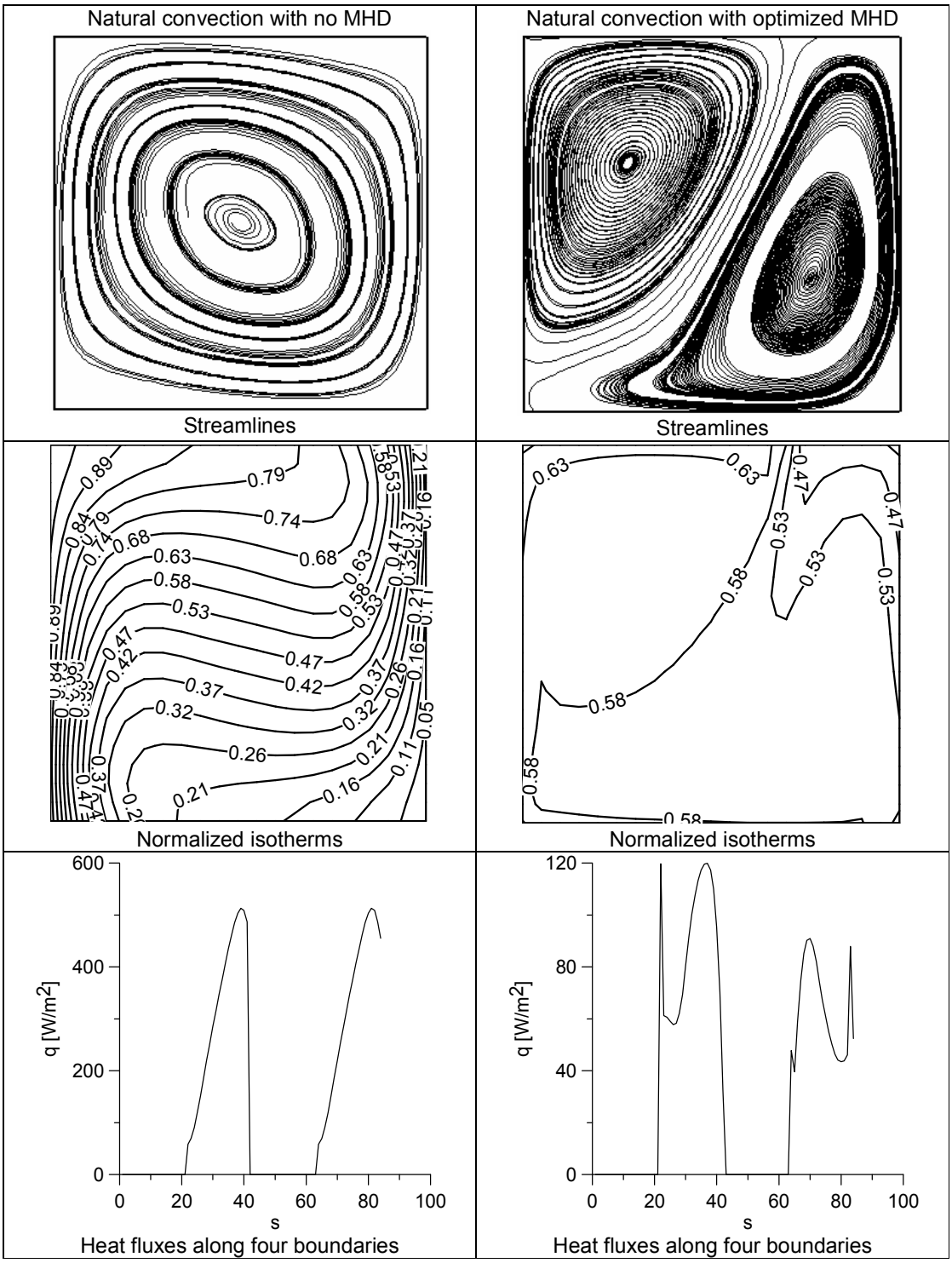

Figure 2. Natural convection; results of analysis with no magnetic field (left column) and results with optimized magnetic boundary conditions (right column) for Ra = 10^5. The parameter *s* is measured counterclockwise along the boundaries of the rectangular container starting from lower left corner.

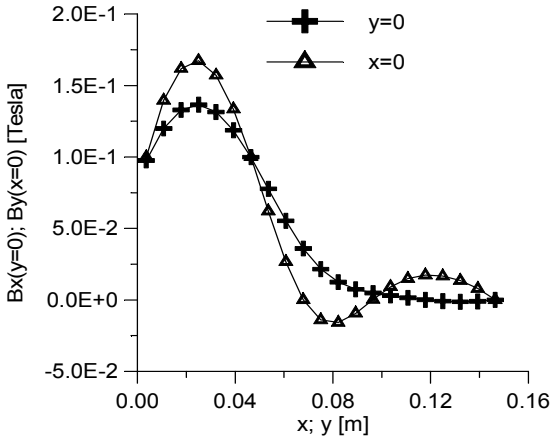

Figure 3. Natural convection; optimized magnetic boundary conditions at $x = 0$ and $y = 0$ with the estimation of **B** at six points per boundary.

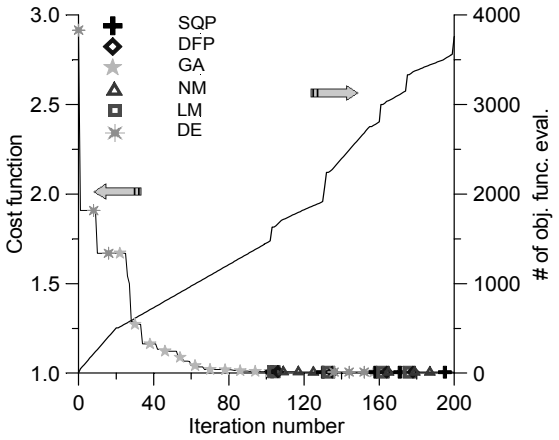

Figure 4. Natural convection; optimization convergence history for the estimation of **B** at six points per boundary.

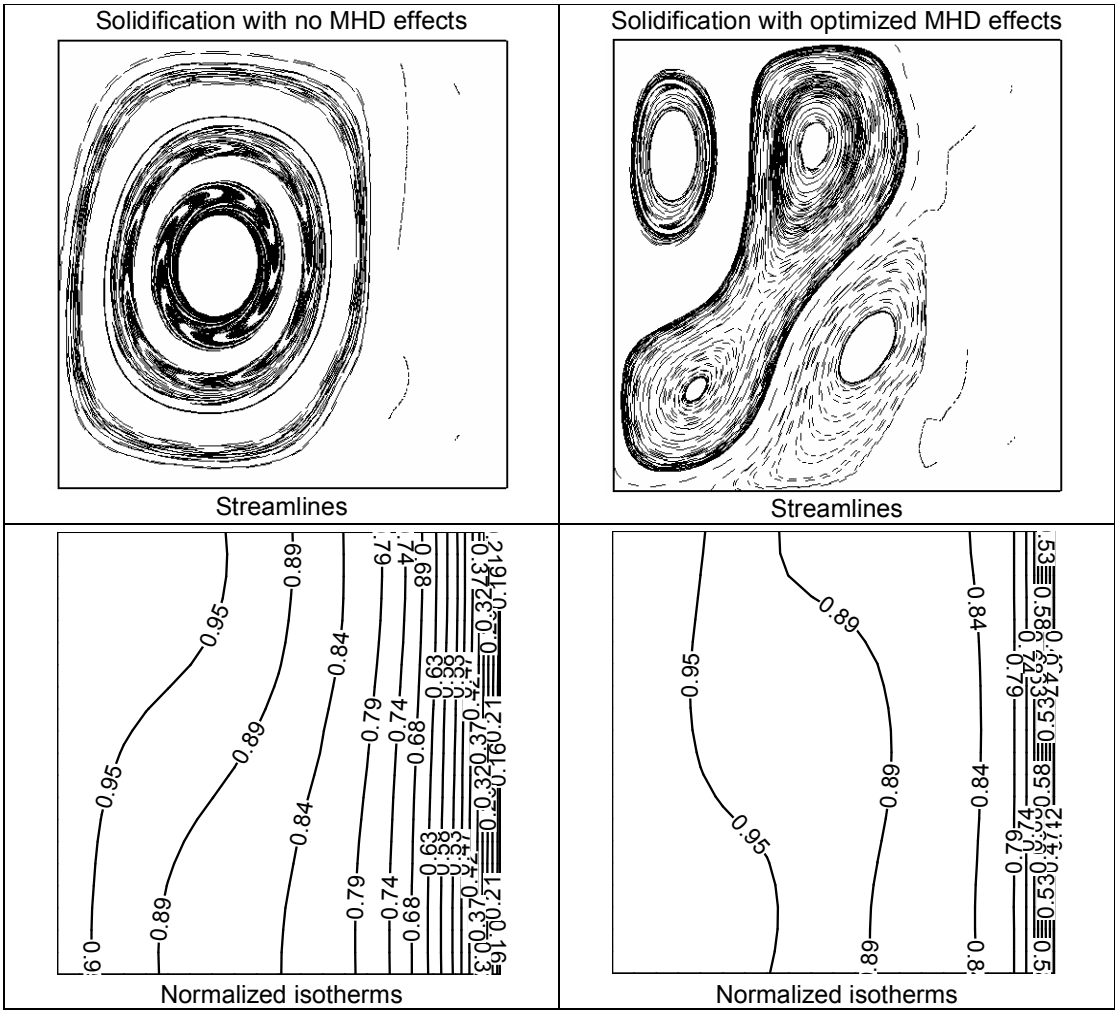

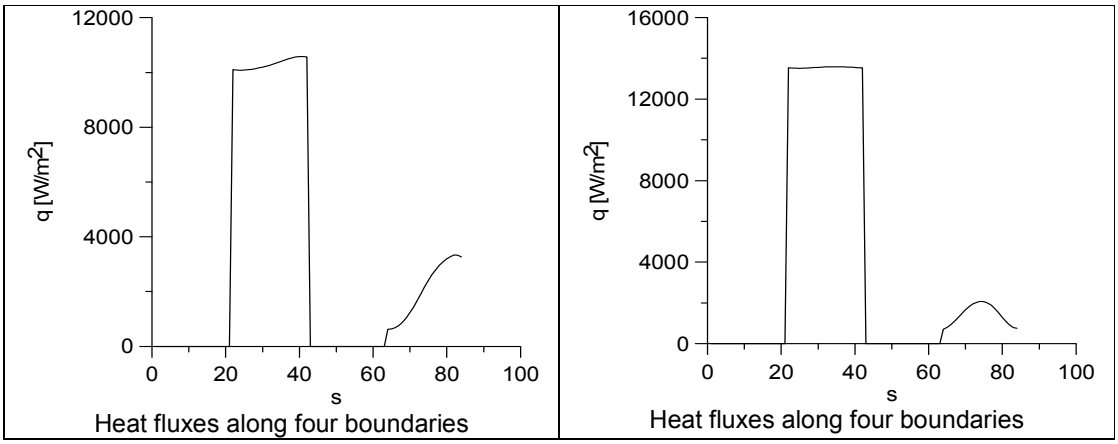

Figure 5. Natural convection with solidification; results of analysis with no magnetic field (left column) and results with optimized magnetic boundary conditions (right column) for Ra = 10^5 . The parameter *s* is measured counterclockwise along the boundaries of the rectangular container starting from lower left corner.

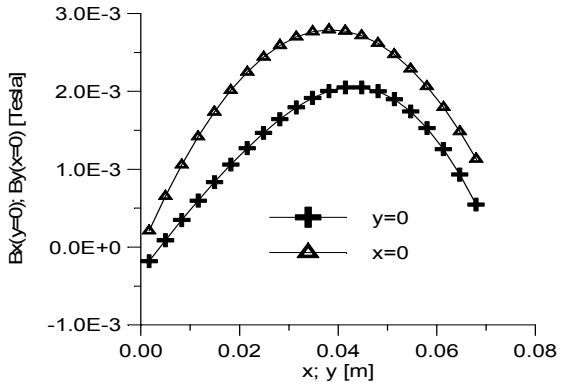

Figure 6. Optimized magnetic boundary conditions on $x = 0$ and $y = 0$ boundaries with the estimation of **B** at six points per boundary in case with solidification.

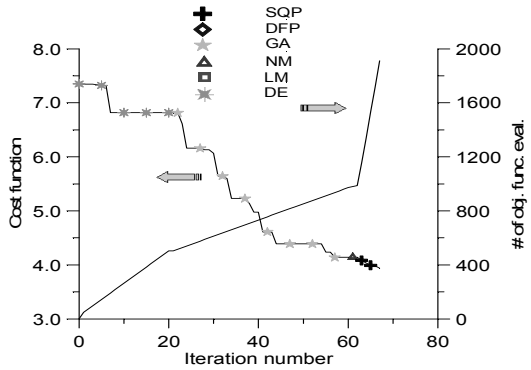

Figure 7. Optimization convergence history for the estimation of **B** at six points per boundary in case with solidification.

.

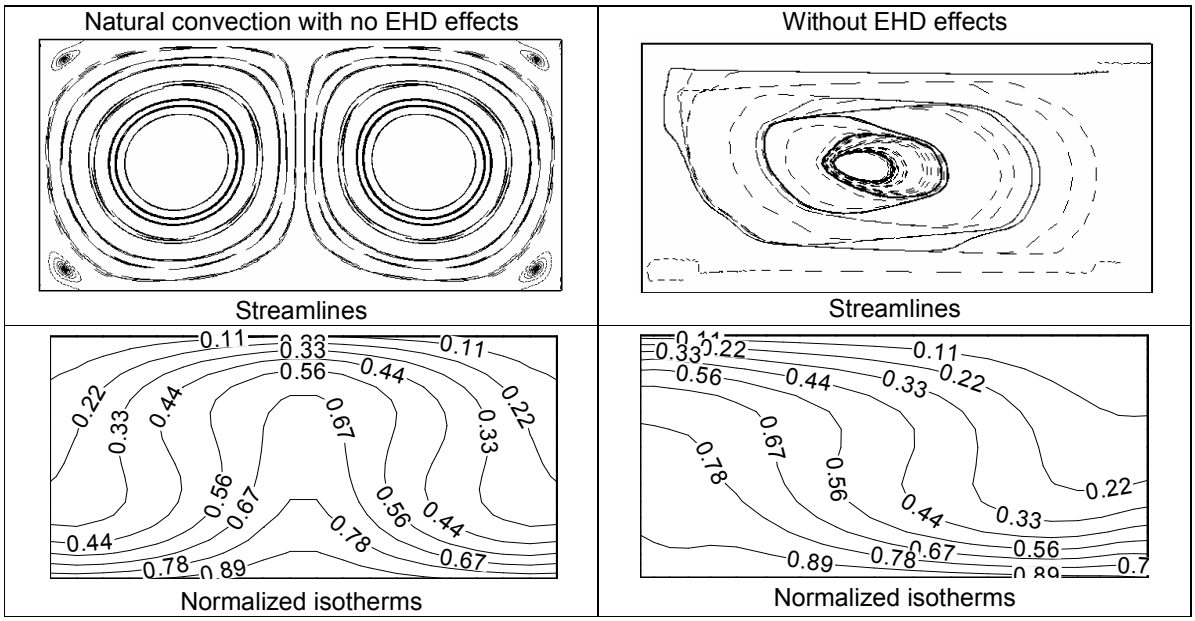

*Adapted from "Instructions for Manuscript Preparations" for ITSS I and Elsevier's "Gateway guide for authors".

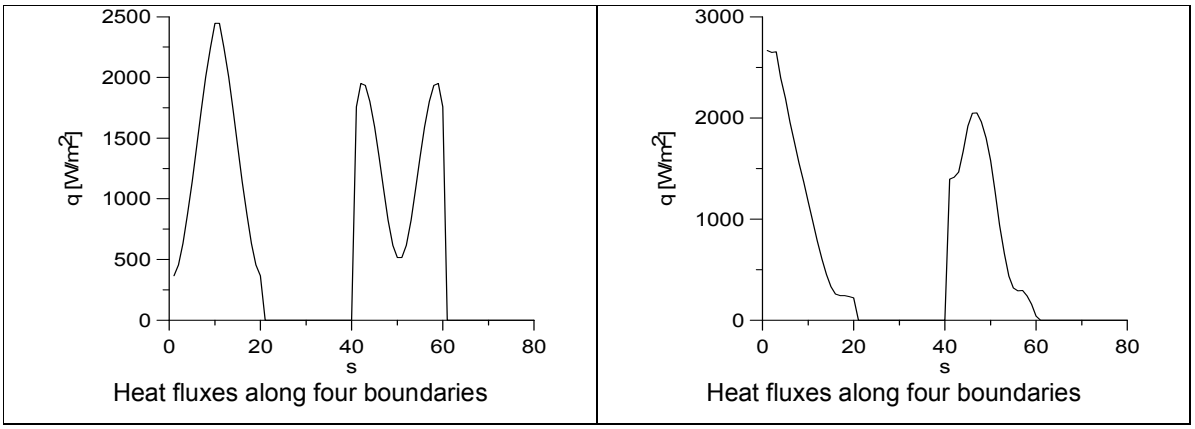

Figure 8. Natural convection with no solidification; results of analysis with no electric field (left column) and results of optimized electric boundary conditions (right column) for Ra = 1.9×10^4 . The parameter *s* is measured counterclockwise along the boundaries of the rectangular container starting from lower left corner.

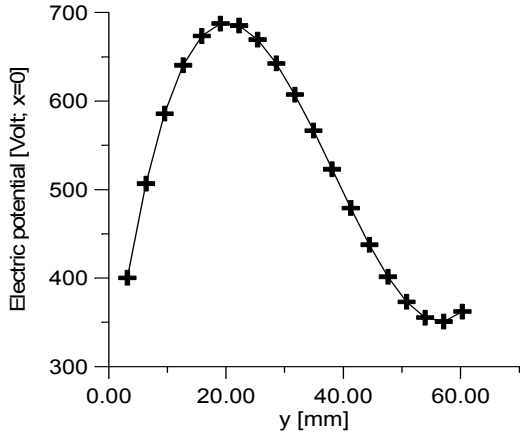

Figure 9. Optimized electric field potential at $x = 0$ and $y = 0$ with the estimation of **E** at six points per boundary.

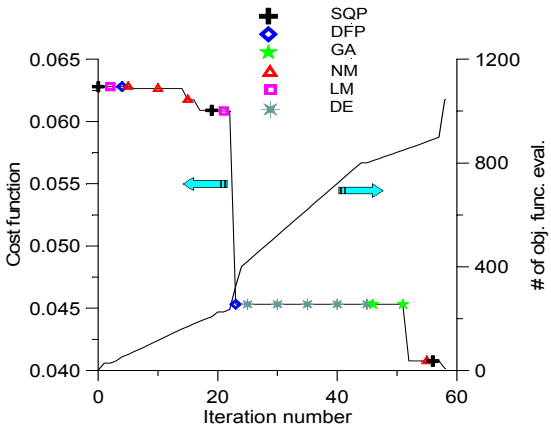

Figure 10. Optimization convergence history for the estimation of **E** at six points per boundary.

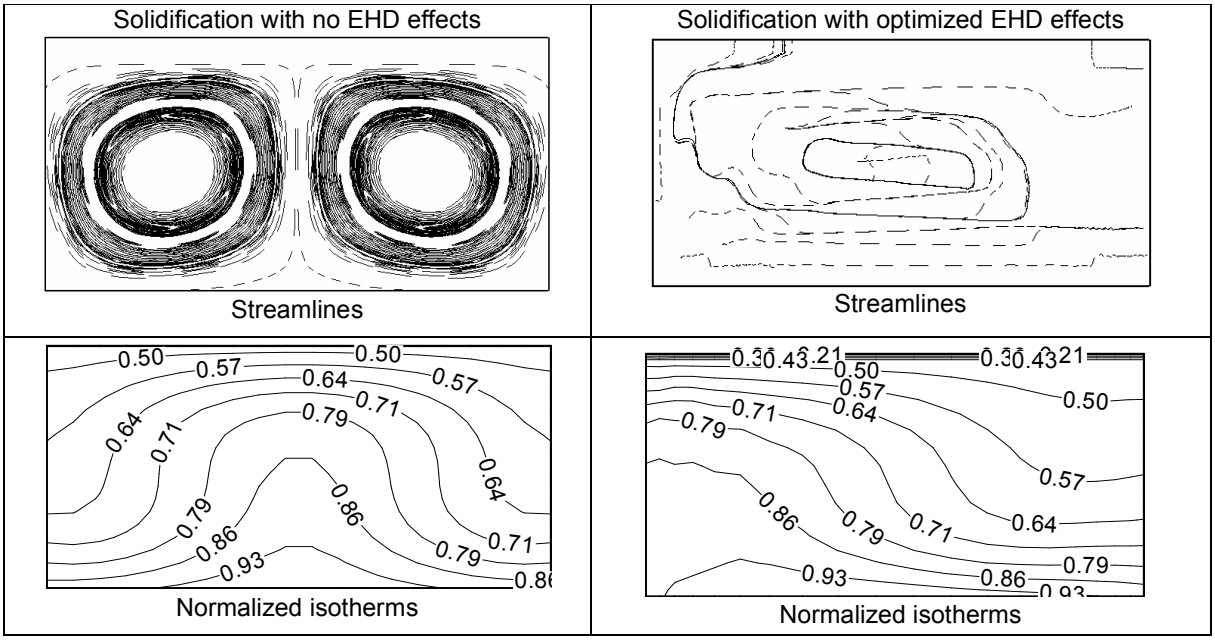

*Adapted from "Instructions for Manuscript Preparations" for ITSS I and Elsevier's "Gateway guide for authors".

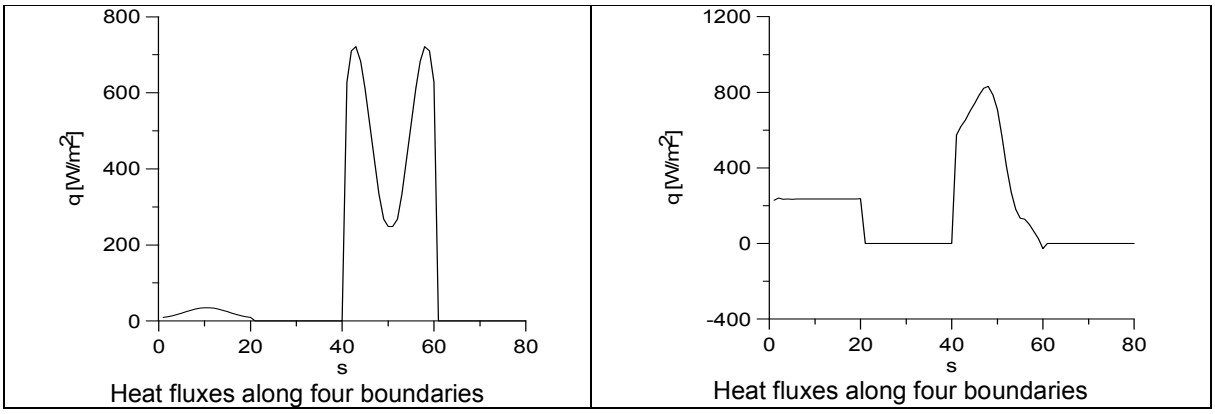

Figure 11. Natural convection with solidification; results of analysis with no electric field (left column) and results of optimized electric boundary conditions (right column) for Ra = 1.9×10^4. The parameter s is measured counterclockwise along the boundaries of the rectangular container starting from lower left corner.

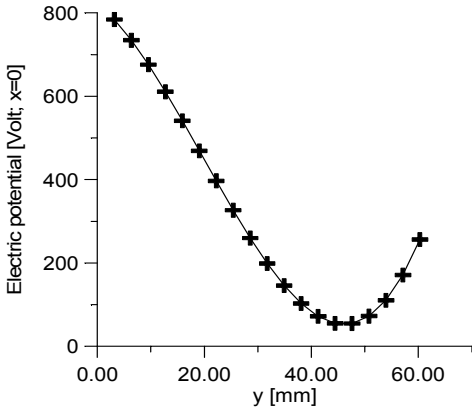

Figure 12. Solidification case: optimized electric potential boundary conditions at $x = 0$ with Ra = 1.9×10^4 and estimation of **E** at six points.

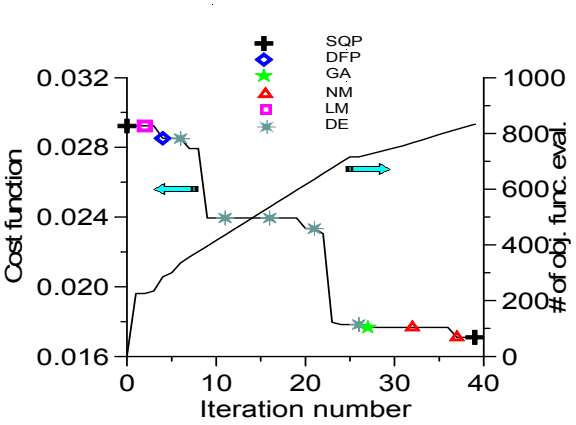

Figure 13. Solidification case: convergence history for Ra = 1.9×10^4 and optimization of **E** at six points at $x = 0$.

Summary

In this paper we showed the results of a time-accurate MHD code that is capable of dealing with phase change problems. The ability to minimize the natural convection effects in problems with and without phase change was demonstrated by utilizing an optimized distribution of magnetic filed along the boundaries of a container. A hybrid constrained optimization algorithm was used in reducing the isotherms pattern to those similar to pure conduction problems.

We have also shown the results of a time-accurate EHD code that is capable of dealing with phase change problems. The ability to minimize the natural convection effects in problems with and without phase change was demonstrated by utilizing an optimized distribution of electric field along the boundaries of a solidification container for the purpose of controlling the solidification process. A hybrid constrained optimization algorithm was used in reducing such natural convection effects.

When space-varying electric potentials were applied, the fluid-flow started to become highly unstable.

For cases where the electric potential was constant along certain wall, such instability did not occur. Further investigations concerning the stability of this type of fluid flow are necessary. However, the concept that it is possible to control the fluid flow and convective heat transfer by the means of an externally applied magnetic and electric field is proved.

Acknowledgements

The first author is grateful for the partial support provided for this research from the grant NSF DMS-0073698 administered through the Computational Mathematics program.

The second author is grateful for the postdoctoral fellowship received from University of Texas at Arlington and from CNPq, a Brazilian council for scientific and technological development.

References

[1] P. Sabhapathy, M.E. Salcudean, Numerical study of flow and heat transfer in LEC growth of GaAs with an axial magnetic field, Journal of Crystal Growth 104 (1990) 371-388.

[2] S. Motakeff, Magnetic field elimination of convective interference with segregation during vertical-Bridgman growth of doped semiconductors, Journal of Crystal Growth 104 (1990) 833-850.

[3] S.-S. Lee, G.S. Dulikravich, B. Kosovic, Electrohydrodynamic (EHD) flow modeling and computations, AIAA Paper 91-1469, AIAA Fluid, Plasma Dynamics and Lasers Conference, Honolulu, Hawaii, June 24-26 (1991).

[4] G.S. Dulikravich, V. Ahuja, S.-S. Lee, Simulation of electrohydrodynamic enhancement of laminar flow heat transfer, Journal of Enhanced Heat Transfer 1 (1) (1993) 115-128.

[5] G.S. Dulikravich, V. Ahuja, Modeling dielectric fluids solidification with charged particles in electric fields and reduced gravity, Numerical Heat Transfer, Fundamentals, Part B, 25 (3) (1994) 357-373.

[6] G.S. Dulikravich, V. Ahuja, S.-S. Lee, Modeling three-dimensional solidification with magnetic fields and reduced gravity, International Journal of Heat and Mass Transfer 37 (5) (1994) 837-853.

[7] G.S. Dulikravich, Electro-Magneto-Hydrodynamics and Solidification, chapter no. 9 in: *Advances in Flow and Rheology of Non-Newtonian Fluids, Part B*, D.A. Siginer, D. De Kee, R.P. Chhabra (Eds.), Rheology Series, 8, Elsevier Publishers, June 1999, pp. 677-716.

[8] B.H. Dennis, G.S. Dulikravich, Simulation of magnetohydrodynamics with conjugate heat transfer, European Congress on Computational Methods in Applied Sciences and Engineering, E. Onate, G. Bugeda, B. Suarez (Eds.), Barcelona, Spain, September 11-14, 2000.

[9] K.I. Fedoseyev, E.J. Kansa, C. Marin, A.G. Ostrogorsky, Magnetic field suppression of semiconductor melt flow in crystal growth: Comparison of three methods for numerical modeling, Japanese CFD Journal 9 (2001) 325 - 333.

[10] A.C. Eringen and G.A. Maugin, *Electrodynamics of Continua II – Fluids and Complex Media*; Springer-Verlag: New York, 1990.

[11] G.S. Dulikravich, S.R. Lynn, Unified electro-magneto-fluid dynamics (EMFD): Introductory concepts, International Journal of Non-Linear Mechanics, 32 (5) (1997) 913-922.

[12] G.S. Dulikravich, S.R. Lynn, Unified electro-magneto-fluid dynamics (EMFD): A survey of mathematical models, International Journal of Non-Linear Mechanics, 32 (5) (1997) 923-932.

[13] H.-J. Ko, G.S. Dulikravich, A fully non-linear model of electro-magneto-hydrodynamics, International J. of Non-Linear Mechanics 35 (4) (2000) 709-719.

[14] G.S. Dulikravich, K.-Y. Choi, S.-S. Lee, Magnetic field control of vorticity in steady incompressible laminar flows, In: Symposium on Developments in Electrorheological Flows and Measurement Uncertainty, ASME FED-Vol. 205/AMD-Vol. 190, pp. 125-142, 1994, D.A. Siginer, J.H. Kim, S.A. Sheriff, H.W. Colleman (Eds.), ASME WAM'94, Chicago, IL, Nov. 6-11, 1994.

[15] R. Sampath, N. Zabaras, Inverse Thermal design of thermo-magnetically driven Boussinesq flows, ASME NHTC00/DAC-1234, Pittsburgh, PA, 2000.

[16] B.H. Dennis, G.S. Dulikravich, Optimization of magneto-hydrodynamic control of diffuser flows using micro-genetic algorithm and least squares finite elements, Journal of Finite Elements in Analysis and Design 37 (5) (2001) 349-363.

[17] B.H. Dennis, G.S. Dulikravich, Magnetic field suppression of melt flow in crystal growth, International Journal of Heat & Fluid Flow 23 (3) (2002) 269-277.

[18] G.S. Dulikravich, M.J. Colaco, T.J. Martin, S.-S. Lee, Magnetized fiber orientation and concentration control in solidifying composites, Journal of Composite Materials 37 (15) (2003) 1351-1366.

[19] M.J. Colaco, G.S. Dulikravich, T.J. Martin, Reducing convection effects in solidification by applying magnetic fields having optimized intensity distribution, ASME paper HT2003-47308, Las Vegas, NV, July 21-23, 2003.

[20] M.J. Colaco, B.H. Dennis, G.S. Dulikravich, T.J. Martin, S.-S. Lee, Optimization of intensities, and orientations of magnets controlling melt flow during solidification, Materials and Manufacturing Processes, 19 (5) (2004).

[21] M.J. Colaco, G.S. Dulikravich, T.J. Martin, Optimization of wall electrodes for electro-hydrodynamic control of natural convection effects during solidification, Materials and Manufacturing Processes, 19 (5) (2004).

[22] V.R. Voller, A.D. Brent, C. Prakash, The modeling of heat, mass and solute transport in solidification systems, International Journal of Heat and Mass Transfer, 32 (1989) 1719-1731.

[23] M. Rappaz, Modelling of microstructure formation in solidification Process. International Materials Reviews 34 (3) (1989) 93-123.

[24] J.P. Van Doormal, G.D. Raithby, Enhancements of the SIMPLE method for predicting incompressible fluid flow, Numer. Heat Transfer 7 (1984) 147-163.

[25] G.D. Raithby, K.E. Torrance, Upstream-weighted differencing schemes and their application to elliptic problems involving fluid flow. Computers & Fluids 2 (1974) 191-206.

[26] G.S. Dulikravich, T.J. Martin, B.H. Dennis, N.F. Foster, Multidisciplinary Hybrid Constrained GA Optimization", chapter 12 in: *EUROGEN'99 - Evolutionary Algorithms in Engineering and Computer Science: Recent Advances and Industrial Applications*, K. Miettinen, M.M. Makela, P. Neittaanmaki, J. Periaux (Eds.), John Wiley & Sons, Jyvaskyla, Finland (1999) 233-259.